Chemical Science

EDGE ARTICLE

View Article Online
View Journal | View Issue

Cite this: *Chem. Sci.*, 2018, **9**, 325

Cooperative loading of multisite receptors with lanthanide containers: an approach for organized luminescent metallopolymers†

Lucille Babel,[a] Laure Guénée,[b] Céline Besnard,[b] Svetlana V. Eliseeva,[c] Stéphane Petoud*[c] and Claude Piguet*[a]

Metal-containing (bio)organic polymers are materials of continuously increasing importance for applications in energy storage and conversion, drug delivery, shape-memory items, supported catalysts, organic conductors and smart photonic devices. The embodiment of luminescent components provides a revolution in lighting and signaling with the ever-increasing development of polymeric light-emitting devices. Despite the unique properties expected from the introduction of optically and magnetically active lanthanides into organic polymers, the deficient control of the metal loading currently limits their design to empirical and poorly reproducible materials. We show here that the synthetic efforts required for producing soluble multi-site host systems ***Lk*** are largely overcome by the virtue of reversible thermodynamics for mastering the metal loading with the help of only two parameters: (1) the affinity of the luminescent lanthanide container for a single binding site and (2) the cooperative effect which modulates the successive fixation of metallic units to adjacent sites. When unsymmetrical perfluorobenzene-trifluoroacetylacetonate co-ligands ($pbta^-$) are selected for balancing the charge of the trivalent lanthanide cations, Ln^{3+}, in six-coordinate $[Ln(pbta)_3]$ containers, the explored anti-cooperative complexation processes induce nearest-neighbor intermetallic interactions $\Delta E_{\mathbf{Lk}}^{Ln(pbta)_3,Ln(pbta)_3}$ twice as large as thermal energy at room temperature ($RT = 2.5$ kJ mol^{-1}). These values have no precedent when using standard symmetrical containers and they pave the way for programming metal alternation in luminescent lanthanidopolymers.

Received 24th August 2017
Accepted 16th October 2017

DOI: 10.1039/c7sc03710d

rsc.li/chemical-science

Introduction

Metal-containing (bio)organic polymers are of the utmost importance in actual daily life and have found a wealth of applications in tailor-made materials for energy storage and energy conversion,[1] drug delivery,[2] shape-memory systems,[3] supported catalysts and organic conductors,[4] smart photonic devices,[5] and modern light-emitting diodes.[6] In the absence of metal, rationalization of the organization of (bio)organic (co) polymers relies on micro-segregation events described by the Huggins–Flory theory of phase demixing,[7] a model which has been recently extended for the programming of thermotropic liquid crystals.[8] The introduction of open-shell transition metals within the polymeric backbone results in novel optical and magnetic properties that are not available in pure organic polymers.[1–5] However, the multifaceted (supra)molecular interactions operating between the polymeric backbone and the metal are at the origin of major difficulties in mastering the formation of metallopolymers with respect to stability, organization, processability and reproducibility. These limitations are even amplified for lanthanidopolymers (*i.e.* lanthanide-containing polymers) because of the versatile coordination behavior of these metallic centers.[5] In order to avoid this pitfall, coordination chemists have restricted the concept of metallopolymers to infinite crystalline assemblies made of anionic ligand strands and cationic nodes forming extended 3D-networks, originally referred to as Wolf-type III metallopolymers[4] or coordination polymers,[9] and nowadays often named metal–organic frameworks (MOFs).[10] These infinite assemblies resemble ionic solids in their essence and lead to robust and inert scaffolds possessing variable porosities. When trivalent emissive lanthanides occupy some nodes of the network, the associated luminescence can be tuned by metal doping[11] or by external stimuli such as temperature jumps or mechanical stress.[12] However, the production of solvent-resistant lanthanidopolymers compatible with partial metal occupancy, specific organization, flexible shaping and adaptable sensing properties is not yet available. Current efforts exploit the empirical mixing of polymeric organic receptors with metallic salts, from which non-soluble adducts are isolated. Their

[a]*Department of Inorganic and Analytical Chemistry, University of Geneva, 30 quai E. Ansermet, CH-1211 Geneva 4, Switzerland. E-mail: Claude.Piguet@unige.ch*

[b]*Laboratory of Crystallography, University of Geneva, 24 quai E. Ansermet, CH-1211 Geneva 4, Switzerland*

[c]*Centre de Biophysique Moléculaire, CNRS UPR 4301, Rue Charles Sadron, F-45071 Orléans Cedex 2, France. E-mail: Stephane.Petoud@cnrs-orleans.fr*

† Electronic supplementary information (ESI) available. CCDC 1551909–1551912. For ESI and crystallographic data in CIF or other electronic format see DOI: 10.1039/c7sc03710d

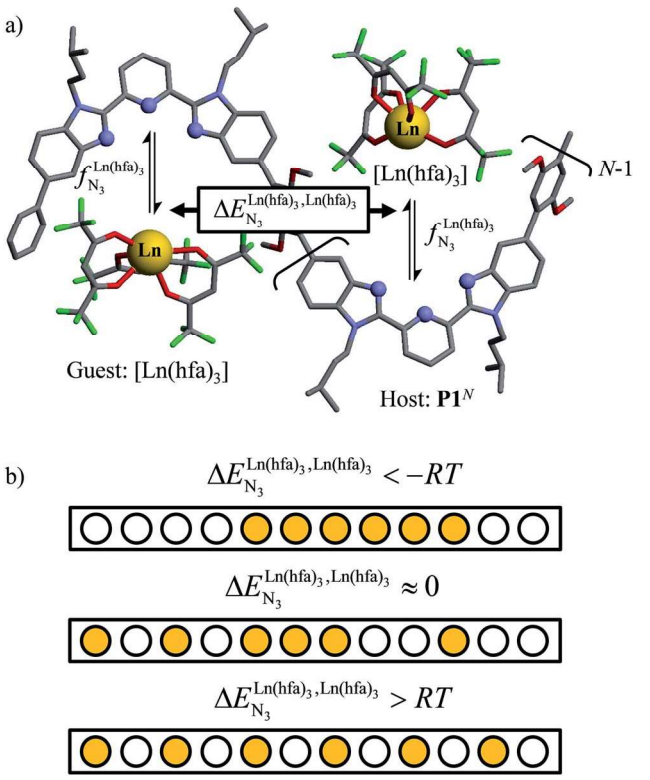

Fig. 1 (a) Thermodynamic model showing successive intermolecular connections of $[Ln(hfa)_3]$ to one-dimensional multi-terdentate receptors $\mathbf{P1}^N$ (N = 10–30).[15] $\Delta G_{N_3}^{Ln(hfa)_3} = -RT \ln(f_{N_3}^{Ln(hfa)_3})$ is the intrinsic intermolecular affinity and $\Delta E_{N_3}^{Ln(hfa)_3,Ln(hfa)_3}$ is the nearest-neighbor interaction (color code: C = grey, N = blue, O = red, F = green, Ln = orange). (b) Pictorial representation of the effect of intermetallic interactions on the microstates of a half-filled metallopolymer (orange disc = occupied site, white disc = empty site).

limited reproducibility and difficult characterization[13] severely restrict pertinent developments along this line. An alternative approach proposes to take advantage of the powerful toolkit of reversible thermodynamics that has been developed to unravel multiple protonations in linear polyelectrolytes,[14] for the in-depth deciphering of the loading of linear polymeric multi-terdentate receptors $\mathbf{P1}^N$ with neutral luminescent $[Ln(hfa)_3]$ complexes (Ln = trivalent lanthanide, hfa = hexafluoroacetylacetonate) in dichloromethane (Fig. 1a).[15] In solution, lanthanide tris-betadiketonate complexes exist as Lewis base adducts $[Ln(hfa)_3$-X] where X is a solvent molecule or an additional donor atom borne by co-ligands. Upon reaction with the target binding site of a polymer, for instance $\mathbf{P1}^N$, only the core $[Ln(hfa)_3]$ is transferred (Fig. 1a). In order to use a single concept for the source $[Ln(hfa)_3X]$ and the transferable core $[Ln(hfa)_3]$, we use the term 'neutral lanthanide container' for describing these beta-diketonate coordination complexes. Using the site-binding model,[14,16] complexation processes can be modeled using two simple parameters: (1) the free energy of the intermolecular affinity of the entering metal for one terdentate N_3 site $\Delta G_{N_3}^{Ln(hfa)_3} = -RT \ln\left(f_{N_3}^{Ln(hfa)_3}\right)$, which is the unique parameter to be considered for a monomeric unit and (2) the inter-site interaction energy $\Delta E_{N_3}^{Ln(hfa)_3,Ln(hfa)_3}$ which accounts for modulations of the intrinsic affinity when multiple binding events operate in binuclear (or higher-order) linear receptors (*i.e.* cooperativity).[17] Whereas major attention is usually focused on the maximization of host-guest affinities (*i.e.* minimizing $\Delta G_{N_3}^{Ln(hfa)_3}$), an instructed programming of $\Delta E_{N_3}^{Ln(hfa)_3,Ln(hfa)_3}$ is more tricky since both negative (cooperative) or positive (anti-cooperative) issues are attractive for specific applications.

For instance, metal clustering compatible with efficient short-range intermetallic communication and energy migration[18]

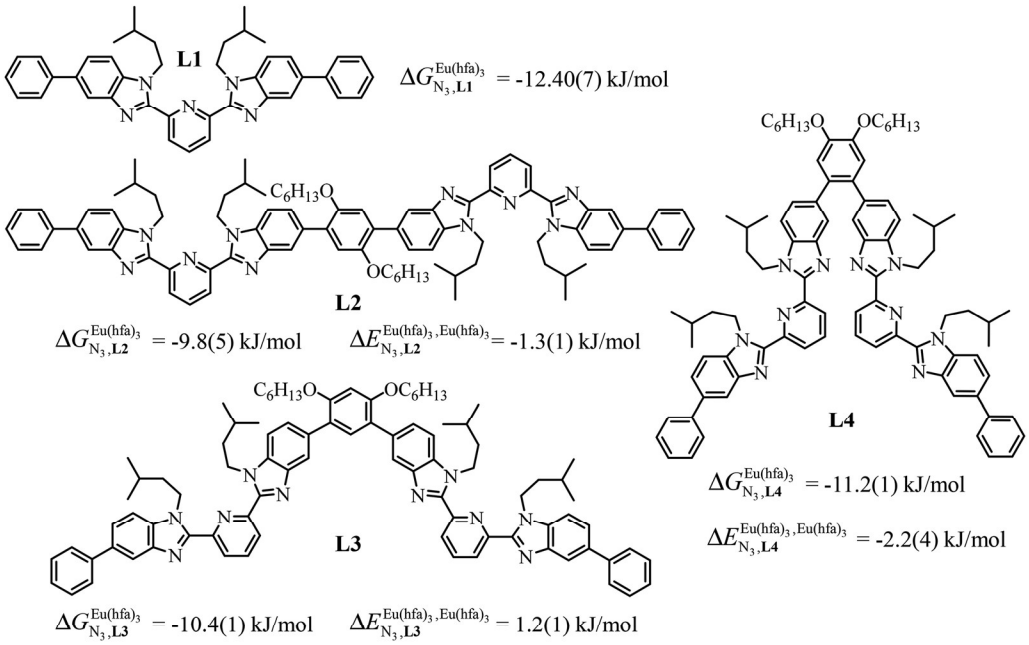

Fig. 2 Chemical structures of ligands L1–L4 gathering the thermodynamic intermolecular affinities $\Delta G_{N_3}^{Eu(hfa)_3}$ and nearest-neighbor interactions $\Delta E_{N_3}^{Eu(hfa)_3,Eu(hfa)_3}$ for their loading with $[Eu(hfa)_3]$ (CD_2Cl_2, 298 K).

results when $\Delta E_{N_3}^{Ln(hfa)_3,Ln(hfa)_3} < -RT$ (cooperative process, top of Fig. 1b). In contrast, metal alternation produced by anti-cooperative processes ($\Delta E_{N_3}^{Ln(hfa)_3,Ln(hfa)_3} > RT$, bottom of Fig. 1b) in half-filled linear metallopolymers is appealing for applications in drug sensing,[19] light-upconversion[20] and metal segregation.[21] Finally, $\Delta E_{N_3}^{Ln(hfa)_3,Ln(hfa)_3} \approx 0$ (middle of Fig. 1b) produces uncontrolled statistical metallic dispersion, a behavior found in most doped MOFs, and which is encountered for metallopolymers possessing large inter-site separations.[14c] The experimental magnitude of the inter-site interaction parameters $0.7 \leq \left|\Delta E_{N_3}^{Ln(hfa)_3,Ln(hfa)_3}\right| \leq 2.3$ kJ mol^{-1} observed for the loading of polymers $\mathbf{P1}^N$ with symmetrical [Ln(hfa)$_3$] containers (Ln = Y, La, Eu and Lu, Fig. 1a) in dichloromethane did not exceed the average thermal energy (RT = 2.5 kJ mol^{-1}), and therefore no organization could be induced on the macroscopic scale.[15]

A recent focus[17] on a family of monomeric **L1** and dimeric model ligands **L2–L4** (Fig. 2) demonstrated that (i) the intrinsic affinities $\Delta G_{N_3}^{Ln(hfa)_3}$ exponentially decrease with the number of binding sites, (ii) the inter-site interactions $\Delta E_{N_3}^{Ln(hfa)_3,Ln(hfa)_3}$ are affected by the relative geometries of the binding sites and (iii) minor changes in solvation processes, well described by the Onsager equation,[22] are responsible for the tuning of these thermodynamic parameters. With these theoretical toolkits in hand, we suspect that the successive fixation of unsymmetrical lanthanide containers [Ln(tfa)$_3$], [Ln(pta)$_3$], [Ln(tta)$_3$] and [Ln(pbta)$_3$], instead of symmetrical [Ln(hfa)$_3$] (Fig. 3), could provide magnified anti-cooperative processes.[17] Taking the same set of ligands **L1–L4** as a proof-of-concept, we report here that unsymmetrical [Ln(pbta)$_3$] follows the predicted trend and exhibits, to the best of our knowledge, the largest intermetallic inter-site interactions ever quantified for neutral polynuclear lanthanide complexes.

Results and discussion

Synthesis and characterization of unsymmetrical neutral lanthanide containers [Ln(tfa)$_3$dig], [Ln(pta)$_3$dig], [Ln(tta)$_3$dig] and [Ln(pbta)$_3$dig]

The desired unsymmetrical lanthanide containers were synthesised following the strategy developed for [Ln(hfa)$_3$dig].[23] Bis(2-methoxyethyl)ether (diglyme = dig) was added to a suspension of either lanthanide oxide Ln_2O_3, hydroxide $Ln(OH)_3 \cdot xH_2O$ or chloride $LnCl_3 \cdot xH_2O$ (combined with 3 eq. NaOH) in aprotic solvent (CH_2Cl_2, hexane or toluene) followed by the addition of the pertinent β-diketonate ligand. Purification by crystallisation or sublimation provided the target products [Ln(X)$_3$dig] (X = pta, tta and pbta) in various yields (Fig. 3 and Appendix 1 in the ESI†). The europium container [Eu(tfa)$_3$dig] could not be obtained and the reaction stopped with the formation of $Eu(tfa)_3 \cdot xH_2O$, probably because the bound anionic diketonate ligands are too strong as donors for releasing sufficient residual positive charge on the lanthanide for further complexation with neutral diglyme. A similar limitation was encountered with pivaloyl-trifluoroacetone (pta) ligands, for which tricky sublimations of intricate mixtures provided only 9% of the target product [Eu(pta)$_3$dig]. The remaining electron-deficient β-diketonate ligands, tta and pbta, gave [Ln(tta)$_3$dig] and [Ln(pbta)$_3$dig] (Ln = La, Eu, and Y) in moderate (Ln = Y) to good (Ln = Eu and La) yields.

The ^{1}H and ^{19}F-NMR spectra confirm the formation of pseudo-C_3 species in solution, which are dynamic on the NMR time scale (Fig. 4 and S1–S4 in the ESI†).[24] Elemental analyses of the microcrystalline powders point to the formation of unsolvated [Ln(β-diketonate)$_3$dig] adducts (Appendix 1), a trend confirmed by the X-ray crystal structures solved for [Eu(tta)$_3$dig] (**1**), [Y(tta)$_3$dig] (**2**) and [Eu(pbta)$_3$dig] (**3**) (Fig. 5, S4–S6 and Tables

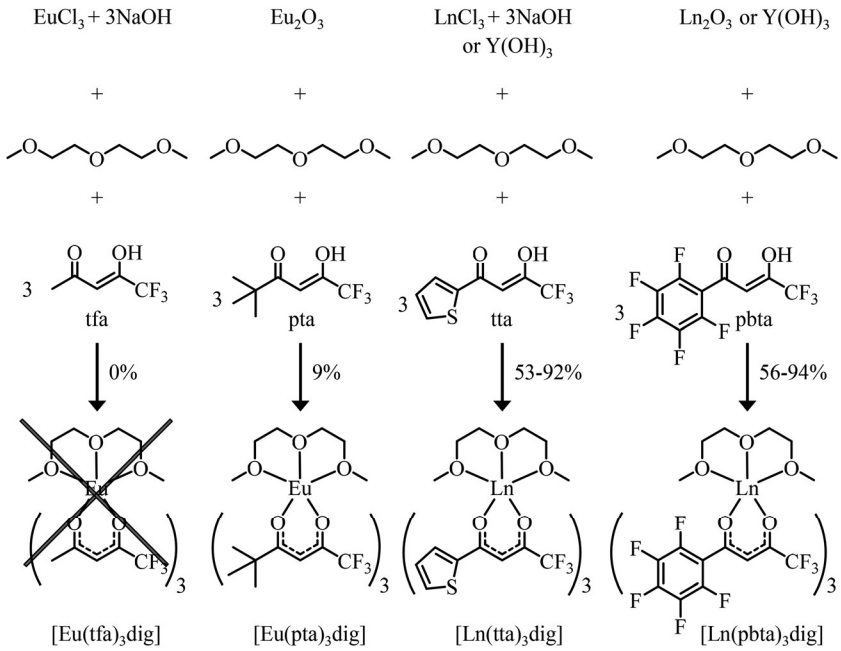

Fig. 3 Reaction pathways for the syntheses of unsymmetrical lanthanide containers.

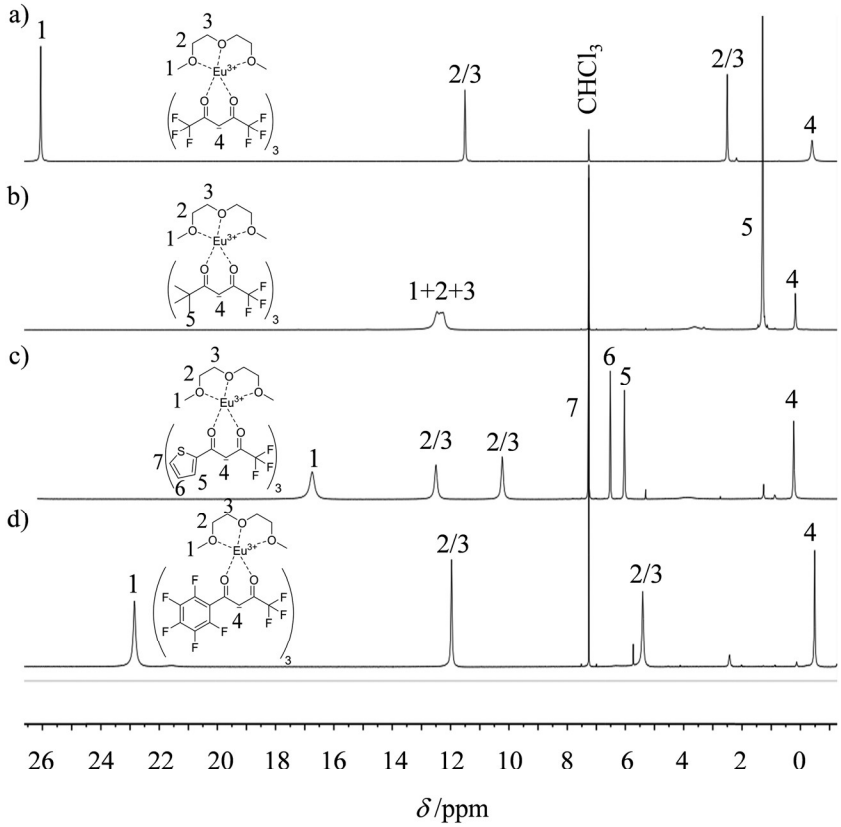

Fig. 4 ^{1}H NMR spectra of europium-containing lanthanide containers (a) [Eu(hfa)$_3$dig], (b) [Eu(pta)$_3$dig], (c) [Eu(tta)$_3$dig] and (d) [Eu(pbta)$_3$dig] with numbering scheme ($CDCl_3$, 298 K).

S1–S13†). All bond lengths in the europium complexes [Eu(tta)$_3$dig] (**1**) and [Eu(pbta)$_3$dig] (**3**) are within the standard range and are comparable to those reported for symmetrical [Eu(hfa)$_3$dig] (Table S13†),[25] a trend in line with similar affinities displayed by any of the fluorinated β-diketonate ligands (hfa^-, tta^- and $pbta^-$) for the central trivalent cation.

Subject to SHAPE[26] analysis, the EuO_9 coordination spheres correspond best to monocapped square antiprisms with the central oxygen donor of the diglyme ligand occupying the capping position (Fig. S7a†). The smaller size of trivalent yttrium leads to eight-coordination in [Y(tta)$_3$dig] (**2**) where the diglyme acts as a bidentate ligand (Fig. 5b). The eight bound oxygen atoms occupy the vertices of an approximate square antiprism,[26] a trend in line with quantum chemical calculations performed on [Y(tta)$_3$(H$_2$O)$_x$] in the gas-phase.[27] Compared with [Eu(tta)$_3$dig] (Fig. 5a), two tta diketonate ligands are significantly twisted in [Y(tta)$_3$dig] (Fig. S8†). All bond valences significantly increase as a result of the larger residual charge carried by the eight-coordinate Y^{III} (Table S13†). The electric dipole moments computed for the gas-phase optimised geometries (Fig. S7b†) roughly point along the Ln–O$_{central}$(diglyme) bond direction and decrease in the order hfa (7.7 D) > pbta (6.7 D) > tta (4.6 D), a tendency which contrasts with pioneer calculations performed for six-coordinate [Ln(β-diketonate)$_3$] systems[28] and with chemical intuition, which naively associates larger dipole moments with unsymmetrical β-diketonate ligands. We conclude that the magnitudes of the dipole moments in [LnX$_3$dig] are indeed controlled by the residual positive charge borne by the trivalent lanthanide, which increases with the electron-withdrawing effect of the bound β-diketonate ligands (hfa > pbta ≫ tta).

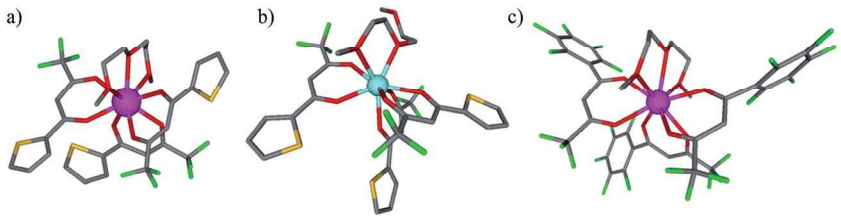

Fig. 5 Molecular structures of (a) [Eu(tta)$_3$dig] (**1**), (b) [Y(tta)$_3$dig] (**2**) and (c) [Eu(pbta)$_3$dig] (**3**) as observed in their crystal structures. Color codes: C = grey, O = red, S = yellow, F = green, Eu = magenta, and Y = light blue. The hydrogen atoms have been omitted for clarity.

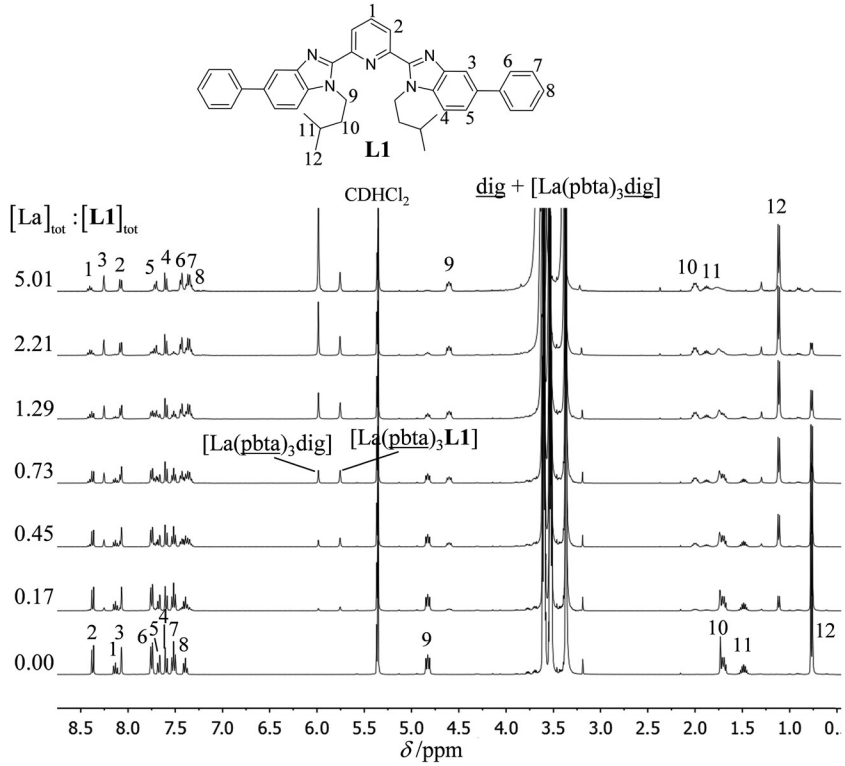

Fig. 6 ^{1}H NMR titration of L1 (10 mM) with [La(pbta)$_3$dig] in CD_2Cl_2 + 0.14 m diglyme at 298 K.

Thermodynamic loading of the terdentate ligand L1 with the unsymmetrical neutral lanthanide containers [Ln(pta)$_3$dig], [Ln(tta)$_3$dig] and [Ln(pbta)$_3$dig]: a strategy for addressing intrinsic intermolecular affinities

The ^{1}H NMR titrations of 10 mm of the monomeric terdentate ligand **L1** with [LnX$_3$dig] (Ln = La, Eu, and Y; X = pta, tta and pbta; dig = diglyme) conducted in dichloromethane containing an excess of diglyme ([dig]$_{tot}$ = 0.14 m) show the formation of a single adduct [LnX$_3$**L1**] complex according to eqn (1) (Fig. 6 and Tables S14 and S15†).[15a]

$$\mathbf{L1} + [\mathrm{LnX_3dig}] \rightleftharpoons [\mathrm{LnX_3}\mathbf{L1}] + \mathrm{dig}\ \beta_{\mathrm{exch},1}^{\mathrm{LnX_3},\mathbf{L1}} = \frac{[\mathrm{LnX_3}\mathbf{L1}]\cdot[\mathrm{dig}]}{[\mathrm{LnX_3dig}]\cdot[\mathbf{L1}]} \quad (1)$$

Since the total concentration of diglyme does not significantly vary, the stability constant $\beta_{\mathrm{exch},1}^{\mathrm{LnX_3},\mathbf{L1}}$ associated with the ligand exchange process depicted in eqn (1) reduces to the conditional association constant $\beta_{\mathrm{cond},1,1}^{\mathrm{LnX_3},\mathbf{L1}}$ summarized in eqn (2), where $f_{\mathbf{L1},\mathrm{cond}}^{\mathrm{LnX_3}}$ is the conditional affinity factor of a terdentate site for a [LnX$_3$] container (Fig. 1a).[15a]

$$\beta_{\mathrm{cond},1,1}^{\mathrm{LnX_3},\mathbf{L1}} = \frac{\beta_{\mathrm{exch},1}^{\mathrm{LnX_3},\mathbf{L1}}}{[\mathrm{dig}]_{\mathrm{tot}}} = \frac{[\mathrm{LnX_3}\mathbf{L1}]}{[\mathrm{LnX_3dig}]\cdot[\mathbf{L1}]} = f_{\mathbf{L1},\mathrm{cond}}^{\mathrm{LnX_3}} \quad (2)$$

Experimentally, the integrations of the ^{1}H NMR signals recorded for a given proton connected either to the free ligand **L1** ($I_{\mathbf{L1}}^{\mathrm{H}}$) or to the coordinate ligand in [LnX$_3$**L1**] ($I_{\mathrm{LnX_3}\mathbf{L1}}^{\mathrm{H}}$) can be combined to determine the occupancy factor $\theta_{\mathrm{Ln}}^{\mathbf{L1}}$ (left part of eqn (3)), which is related to the association constant $\beta_{\mathrm{cond},1,1}^{\mathrm{LnX_3},\mathbf{L1}}$ *via* the Langmuir binding isotherm (right part of eqn (3)).[15a]

$$\theta_{\mathrm{Ln}}^{\mathbf{L1}} = \frac{[\mathrm{Ln}]_{\mathrm{bound}}}{[\mathbf{L1}]_{\mathrm{tot}}} = \frac{I_{\mathbf{L1}\mathrm{LnX_3}}^{\mathrm{H}}}{I_{\mathbf{L1}}^{\mathrm{H}} + I_{\mathrm{LnX_3}\mathbf{L1}}^{\mathrm{H}}} = \frac{[\mathrm{Ln}]_{\mathrm{tot}} - [\mathrm{LnX_3dig}]}{[\mathbf{L1}]_{\mathrm{tot}}} = \frac{\beta_{\mathrm{cond},1,1}^{\mathrm{LnX_3},\mathbf{L1}}[\mathrm{LnX_3dig}]}{1 + \beta_{\mathrm{cond},1,1}^{\mathrm{LnX_3},\mathbf{L1}}[\mathrm{LnX_3dig}]} \quad (3)$$

Repeating this procedure for different $\langle[\mathbf{L1}]_{\mathrm{tot}};[\mathrm{Ln}]_{\mathrm{tot}}\rangle$ ratios (Fig. 6) yields occupancy factors $\theta_{\mathrm{Ln}}^{\mathbf{L1}}$ (eqn (3), left) for various free concentrations of the lanthanide container [LnX$_3$dig] (eqn (3), middle). Plots of $\theta_{\mathrm{Ln}}^{\mathbf{L1}}$ related to log([LnX$_3$dig]) (Fig. 7), often referred to as binding isotherms, are fit to eqn (3) (right part) using non-linear least-square techniques to give the conditional association constant $\beta_{\mathrm{cond},1,1}^{\mathrm{LnX_3},\mathbf{L1}} = f_{\mathbf{L1},\mathrm{cond}}^{\mathrm{LnX_3}}$ collected in Table S16† and the intrinsic exchange affinities $\Delta G_{\mathrm{N_3},\mathbf{L1}}^{\mathrm{LnX_3}} = -RT\ln(f_{\mathbf{L1},\mathrm{cond}}^{\mathrm{LnX_3}}\cdot[\mathrm{dig}]_{\mathrm{tot}}) = -RT\ln(f_{\mathbf{L1}}^{\mathrm{LnX_3}})$ depicted in Fig. 8.

For the unsymmetrical perfluorobenzene-trifluoroacetylacetonate lanthanide containers [Ln(pbta)$_3$dig] (Ln = La, Eu, and Y, the blue traces in Fig. 7 and 8), the intrinsic exchange affinities $\Delta G_{\mathrm{N_3},\mathbf{L1}}^{\mathrm{LnX_3}}$ (eqn (1)) increase by 8–14% with respect to those found for the famous symmetrical [Ln(hfa)$_3$dig] analogues (red traces in Fig. 7 and 8). For the unsymmetrical, but less electron-deficient thienyl-trifluoroacetylacetonato lanthanide containers [Ln(tta)$_3$dig] (Ln = La, Eu, and Y, the green traces in Fig. 7 and 8), the affinity for **L1** is still detectable, but low enough when Ln = Y for providing fast exchange on the NMR scale. In these conditions, the monitoring of a single

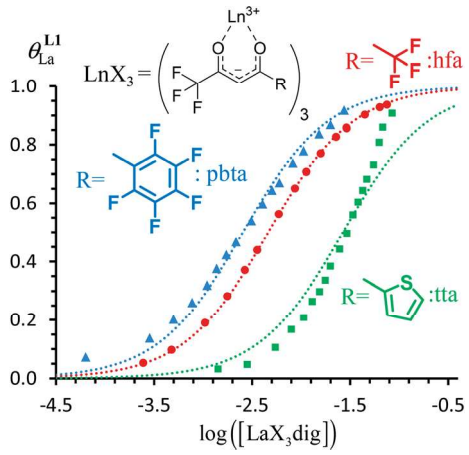

Fig. 7 Binding isotherms built from ^{1}H NMR titrations of **L1** with [LaX_3dig] (X = hfa (red), tta (green) or pbta (blue)) in CD_2Cl_2 + 0.14 m dig at 293 K. The dotted traces correspond to the fitted curves computed with eqn (3) and using $\beta_{cond,1,1}^{LnX_3,L1}$ collected in Table S16.†

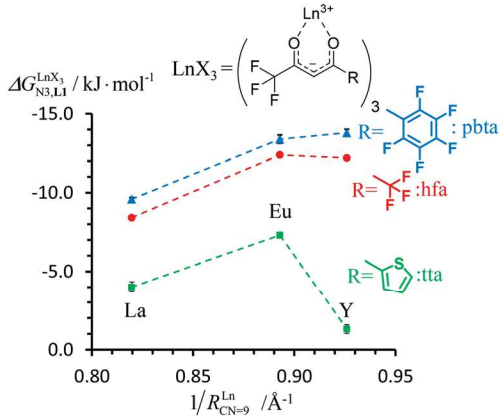

Fig. 8 Intrinsic exchange affinities $\Delta G_{N_3,L1}^{LnX_3} = -RT\ \ln(f_{L1,cond}^{LnX_3} \cdot [dig]_{tot}) = -RT\ \ln(f_{L1}^{LnX_3})$ for the loading of monomeric ligand **L1** with [Ln(hfa)$_3$dig] (red), [Ln(tta)$_3$dig] (green) and [Ln(pbta)$_3$dig] (blue) in CD_2Cl_2 at 298 K. $1/R_{CN=9}^{Ln}$ is the inverse of the nine-coordinate lanthanide radius. The dotted trend lines are provided as guides.

broadened ^{1}H NMR signal δ_{obs}^{H} for each proton in solution during the titration prevents the use of eqn (3), which is replaced by eqn (4) for estimating the occupancy factor θ_Y^{L1} (δ_{L1}^{H} and $\delta_{Y(tta)_3L1}^{H}$ stand for the chemical shifts of the same proton in pure **L1** and [Y(tta)$_3$**L1**], respectively).

$$\theta_Y^{L1} = \frac{[Y]_{bound}}{[L1]_{tot}} = \frac{[Y(tta)_3L1]}{[L1]_{tot}} = \frac{\delta_{obs}^{H} - \delta_{L1}^{H}}{\delta_{Y(tta)_3L1}^{H} - \delta_{L1}^{H}} = \frac{\beta_{cond,1,1}^{Y(tta)_3,L1}[Y(tta)_3dig]}{1 + \beta_{cond,1,1}^{Y(tta)_3,L1}[Y(tta)_3dig]} \quad (4)$$

For these [Ln(tta)$_3$] containers, occupancy factors larger than 20% are only obtained in a large excess of [Ln(tta)$_3$dig], the total concentrations of which may reach 0.1 M in solution. The express requisite for using an invariant total concentration of diglyme in eqn (2) is no more obeyed and deviations from simple Langmuir isotherms are observed (green trace in Fig. 7). The conditional association constants reported for [Ln(tta)$_3$**L1**] complexes are therefore only mere estimations. Finally, the pyvaloyl-trifluoroacetylacetonate europium container [Eu(pta)$_3$dig], which bears the lowest residual positive charge on the metal,[29] displayed no measurable affinity for **L1** in CD_2Cl_2 at millimolar concentrations, a result in line with the lack (to the best of our knowledge) of crystal structures reporting a nine-coordinate [Ln(pta)$_3$**L**] adduct, where **L** is a terdentate chelate nitrogen donor ligand.[30] Leaving pta-based complexes aside, pure [Ln(pbta)$_3$**L1**] (Ln = La, Eu, and Y) and [Ln(tta)$_3$**L1**] (Ln = La and Eu) complexes could be isolated as crystalline materials from concentrated solutions in 41–92% yield (Appendix 1, Tables S13, S14 and S17†). The crystal structure of [Eu(pbta)$_3$**L1**]·CH_2Cl_2 (**4**) confirms nine-coordination around the europium cation by the three nitrogen atoms of the bound aromatic ligand and the six oxygen atoms of the three bidentate pbta anions (Fig. 9, Tables S18–S21 and Fig. S9†). The [EuN_3O_6] chromophore adopts a distorted monocapped square antiprism geometry,[26] very similar to that previously described for [La(hfa)$_3$**L1**] (Table S22 and Fig. S10†).[15a]

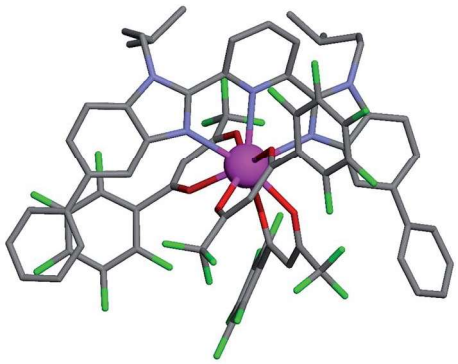

Fig. 9 Molecular structure of [Eu(pbta)$_3$**L1**] found in the crystal structure of [Eu(pbta)$_3$**L1**]·CH_2Cl_2 (**4**). Color codes: C = grey, O = red, F = green, and Eu = magenta. The hydrogen atoms have been omitted for clarity.

In conclusion, two strong electron-withdrawing groups per β-diketonate in hfa (two CF_3 groups) or in pbta (CF_3 and C_6F_5) are required in order to get intrinsic affinities $\Delta G_{N_3,L1}^{LnX_3}$ large enough to form significant amounts of [LnX_3**L1**] at millimolar concentrations (Fig. 8, X represents the β-diketonate anion). The connections of less electron-withdrawing thenoyl (X = tta) or pivaloyl groups (X = pta) are detrimental in terms of the global stabilities of the adducts. This trend is correlated with the dipole moments computed for the gas-phase optimized [YX_3**L1**] complexes, which reveal that the global asymmetry of the charge distribution increases along the series [Y(pbta)$_3$**L1**] (μ = 13.1 D) ≈ [Y(hfa)$_3$**L1**] (μ = 13.8 D) < [Y(tta)$_3$**L1**] (μ = 14.9 D, Fig. S11†).

Thermodynamic loading of multi-terdentate ligands L2–L4 with unsymmetrical neutral lanthanide containers [Eu(tta)$_3$dig] and [Eu(pbta)$_3$dig]: a strategy for addressing nearest-neighbor interactions

A reliable analysis of the inter-site interactions $\Delta E_{\mathbf{L}k}^{\mathrm{LnX_3,LnX_3}}$, which control the successive binding of two adjacent [LnX$_3$] containers in linear multi-site receptors, requires the investigation of the dimeric receptors **L2–L4** (eqn (5) and (6)), for which the cumulative conditional association constants $\beta_{\mathrm{cond},m,1}^{\mathrm{LnX_3},\mathbf{L}k}$ are given in eqn (7) and (8).

$$\mathbf{L}k + [\mathrm{LnX_3dig}] \rightleftharpoons [\mathrm{LnX_3}\mathbf{L}k] + \mathrm{dig}\ \beta_{\mathrm{exch},1}^{\mathrm{LnX_3},\mathbf{L}k} = \frac{[\mathrm{LnX_3}\mathbf{L}k]\cdot[\mathrm{dig}]}{[\mathrm{LnX_3dig}]\cdot[\mathbf{L}k]} \tag{5}$$

$$\mathbf{L}k + 2[\mathrm{LnX_3dig}] \rightleftharpoons [\mathrm{Ln_2X_6}\mathbf{L}k] + 2\mathrm{dig}\ \beta_{\mathrm{exch},2}^{\mathrm{LnX_3},\mathbf{L}k} = \frac{[\mathrm{Ln_2X_6}\mathbf{L}k]\cdot[\mathrm{dig}]^2}{[\mathrm{LnX_3dig}]^2\cdot[\mathbf{L}k]} \tag{6}$$

$$\beta_{\mathrm{cond},1,1}^{\mathrm{LnX_3},\mathbf{L}k} = \frac{\beta_{\mathrm{exch},1}^{\mathrm{LnX_3},\mathbf{L}k}}{[\mathrm{dig}]_{\mathrm{tot}}} = \frac{[\mathrm{LnX_3}\mathbf{L}k]}{[\mathrm{LnX_3dig}]\cdot[\mathbf{L}k]} = 2f_{\mathbf{L}k,\mathrm{cond}}^{\mathrm{LnX_3}} \tag{7}$$

$$\beta_{\mathrm{cond},2,1}^{\mathrm{LnX_3},\mathbf{L}k} = \frac{\beta_{\mathrm{exch},2}^{\mathrm{LnX_3},\mathbf{L}k}}{([\mathrm{dig}]_{\mathrm{tot}})^2} = \frac{[\mathrm{Ln_2X_6}\mathbf{L}k]}{[\mathrm{LnX_3dig}]^2\cdot[\mathbf{L}k]} = \left(f_{\mathbf{L}k,\mathrm{cond}}^{\mathrm{LnX_3}}\right)^2 \mathrm{e}^{-\left(\frac{\Delta E_{\mathbf{L}k}^{\mathrm{LnX_3,LnX_3}}}{RT}\right)} = \left(f_{\mathbf{L}k,\mathrm{cond}}^{\mathrm{LnX_3}}\right)^2 u_{\mathbf{L}k}^{\mathrm{LnX_3,LnX_3}} \tag{8}$$

According to the site binding model,[16] $\beta_{\mathrm{cond},1,1}^{\mathrm{LnX_3},\mathbf{L}k}$ (eqn (7)) reflects the intrinsic binding affinity of the lanthanide container for a single terdentate site, but modulated by a statistical factor of 2 in a dimer. With this in mind, $\beta_{\mathrm{cond},2,1}^{\mathrm{LnX_3},\mathbf{L}k}$ (eqn (8)) easily provides an estimation of the inter-site interactions measured as their Boltzmann factors $u_{\mathbf{L}k}^{\mathrm{LnX_3,LnX_3}} = \exp(-\Delta E_{\mathbf{L}k}^{\mathrm{LnX_3,LnX_3}}/RT) = 4\beta_{\mathrm{cond},2,1}^{\mathrm{LnX_3},\mathbf{L}k}/(\beta_{\mathrm{cond},1,1}^{\mathrm{LnX_3},\mathbf{L}k})^2$, a parameter often referred to as the allosteric cooperativity factor.[31] As the intrinsic affinity of [Ln(tta)$_3$dig] for the terdentate binding unit is too weak to produce significant quantities of the binuclear [Ln$_2$(tta)$_6$**L**k] complexes at millimolar concentrations, the thermodynamic studies performed on the symmetrical [Eu$_2$(hfa)$_6$**L**k] dimers[17] are completed here with the recording of ^{1}H and ^{19}F NMR spectra for the complexation of **L2–L4** (5 mm) with [Eu(pbta)$_3$dig] in CD_2Cl_2 + 0.14 m diglyme (Fig. S12†). The integrations of the various signals (I^{H} and I^{F}) gave occupancy factors (eqn (9) and Fig. 10), which could be fitted to eqn (10) to get the intrinsic affinities $f_{\mathbf{L}k,\mathrm{cond}}^{\mathrm{EuX_3}}$ and cooperativity factors $u_{\mathrm{N_3}}^{\mathrm{EuX_3,EuX_3}}$ collected in Fig. 11 (Table S23†).

$$\theta_{\mathrm{Ln}}^{\mathrm{exp}} = \frac{\langle m\rangle}{N} = \frac{1}{2}\frac{|\mathrm{Ln}|_{\mathrm{bound}}}{|\mathbf{L}k|_{\mathrm{tot}}} = \frac{1}{2}\cdot\frac{I_{\mathrm{LnL}k}^{\mathrm{H}} + 2\left(I_{\mathrm{Ln_2L}k}^{\mathrm{H}}\right)}{I_{\mathbf{L}k}^{\mathrm{H}} + I_{\mathrm{LnL}k}^{\mathrm{H}} + I_{\mathrm{Ln_2L}k}^{\mathrm{H}}} = \frac{I_{\mathrm{LnL}k}^{\mathrm{F}} + I_{\mathrm{Ln_2L}k}^{\mathrm{F}}}{I_{\mathrm{Ln}}^{\mathrm{F}} + I_{\mathrm{LnL}k}^{\mathrm{F}} + I_{\mathrm{Ln_2L}k}^{\mathrm{F}}}\cdot\frac{[\mathrm{Ln}]_{\mathrm{tot}}}{2[\mathbf{L}k]_{\mathrm{tot}}} \tag{9}$$

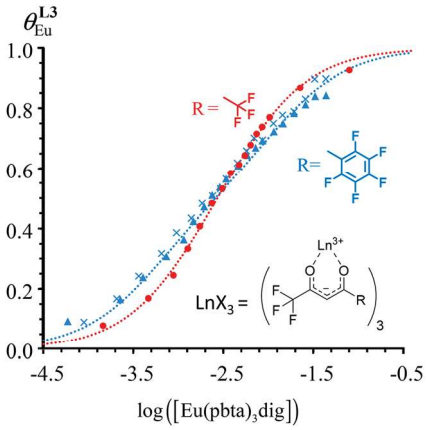

Fig. 10 Occupancy factors and binding isotherms built from NMR titrations of **L3** with [Eu(hfa)$_3$dig] (red disks, ^{1}H NMR)[17] and [Eu(pbta)$_3$dig] (blue triangles for ^{1}H NMR, blue crosses for ^{19}F NMR) in CD_2Cl_2 + 0.14 m dig at 298 K. The dotted traces correspond to the fitted curves computed with eqn 10 and using $f_{\mathbf{L}k,\mathrm{cond}}^{\mathrm{EuX_3}}$ and $u_{1-2}^{\mathrm{EuX_3,EuX_3}}$ collected in Table S23.†

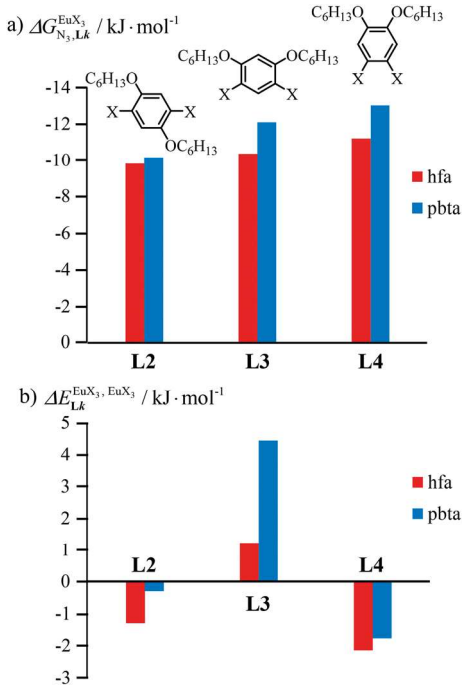

Fig. 11 (a) Intrinsic exchange affinities $\Delta G_{\mathrm{N_3},\mathbf{L}k}^{\mathrm{EuX_3}} = -RT\ \ln(f_{\mathbf{L}k}^{\mathrm{EuX_3}})$ and (b) intermetallic interactions $\Delta E_{\mathbf{L}k}^{\mathrm{EuX_3,EuX_3}} = -RT\ \ln(u_{\mathbf{L}k}^{\mathrm{EuX_3,EuX_3}})$ for the loading of dimeric ligands **L2–L4** (geometries of the spacers are highlighted) with [Eu(hfa)$_3$dig] (red) and [Eu(pbta)$_3$dig] (blue) (CD_2Cl_2, 298 K).

$$\theta_{\mathrm{Ln}}^{\mathrm{calcd}} = \frac{1}{2}\frac{|\mathrm{Ln}|_{\mathrm{bound}}}{|\mathbf{L}k|_{\mathrm{tot}}} = \frac{[\mathrm{LnX_3}\mathbf{L}k] + 2[\mathrm{Ln_2X_6}\mathbf{L}k]}{2[\mathbf{L}k]_{\mathrm{tot}}} = \frac{1}{2}\left(\frac{2f_{\mathbf{L}k,\mathrm{cond}}^{\mathrm{LnX_3}}[\mathrm{Ln}] + 2\left(f_{\mathbf{L}k,\mathrm{cond}}^{\mathrm{LnX_3}}\right)^2 u_{1-2}^{\mathrm{LnX_3,LnX_3}}[\mathrm{Ln}]^2}{1 + 2f_{\mathbf{L}k,\mathrm{cond}}^{\mathrm{LnX_3}}[\mathrm{Ln}] + \left(f_{\mathbf{L}k,\mathrm{cond}}^{\mathrm{LnX_3}}\right)^2 u_{1-2}^{\mathrm{LnX_3,LnX_3}}[\mathrm{Ln}]^2}\right) \tag{10}$$

In line with the trend observed for the monomeric ligand **L1** (Fig. 8), the intrinsic affinities of a terdentate unit in the dimeric ligands **L2–L4** are roughly 10% larger for [Eu(pbta)$_3$dig] than for [Eu(hfa)$_3$dig] (Fig. 11a). The observed intermetallic interactions $\Delta E_{Lk}^{EuX_3,EuX_3}$ are systematically shifted toward more anti-cooperative processes for [Eu$_2$(pbta)$_6$**L***k*] complexes (Fig. 11b).

This drift culminates for [Eu$_2$(pbta)$_6$**L3**], in which the anti-cooperative interaction between the two unsymmetrical [Eu(pbta)$_3$] containers amounts to almost +5 kJ mol^{-1}, a value which should prevent a statistical redistribution due to thermal energy in half-filled linear polymers integrating this bis-terdentate structural motif. Considering that (i) the intermetallic distances are similar in the structures of [Eu$_2$(hfa)$_3$**L3**] (Eu⋯Eu = 12.61 Å in its crystal structure)[17] and [Eu$_2$(pbta)$_3$**L3**] and (ii) the dipole moment calculated for [Y(pbta)$_3$**L1**] is only slightly smaller than that found for [Eu(hfa)$_3$**L1**] (Fig. S11†), we assign the gain in intermetallic repulsion by a factor of 3.7(6), going from [Eu$_2$(hfa)$_3$**L3**] (symmetrical β-diketonate) to [Eu$_2$(pbta)$_3$**L3**] (unsymmetrical β-diketonate), to specific solvation effects which are known to largely dominate over the minor contributions produced by intramolecular dipole–dipole interactions.[17]

Photophysical properties and luminescence quantum yields of the europium containers [EuX$_3$(dig)] (X = hfa, tta, pbta) and of their mononuclear [EuX$_3$**L1**] and binuclear [Eu$_2$(hfa)$_6$L*k*] complexes (L*k* = L2–L4)

The electronic absorption spectra of the europium containers [EuX$_3$(dig)] (X = hfa, tta, and pbta) are dominated by β-diketonate-centred π* ← π transitions occurring in the near-UV range (dotted traces in Fig. 12 and S13†). The maximum of the absorption envelope is shifted stepwise toward lower energy upon the replacement of the trifluoromethyl substituents found in [Eu(hfa)$_3$dig] (33 100 cm^{-1}, Fig. S13†) with aromatic groups in [Eu(pbta)$_3$dig] (32 000 cm^{-1} for one pentafluorobenzene unit, Fig. 12b) and [Eu(tta)$_3$dig] (30 000 cm^{-1} for one thenoyl unit, Fig. 12a). Exchanging the saturated diglyme ligand with the aromatic terdentate ligand **L1** in [EuX$_3$**L1**] provides absorption spectra (full traces in Fig. 12) which combine the contributions of each individual chromophore, *i.e.* the β-diketonate-centred π* ← π transitions (dotted traces in Fig. 12) together with **L1**-centered $^1\pi^*_{L1} \leftarrow {}^1\pi_{1,L1}$ and $^1\pi^*_{L1} \leftarrow {}^1\pi_{2,L1}$ transitions (dashed traces in Fig. 12).[32] Room-temperature excitations ($\tilde{\nu}_{exc}$ = 26 000–30 000 cm^{-1}) of the [EuX$_3$dig] or [EuX$_3$**L1**] complexes (X = hfa, tta, and pbta) in solution (Fig. 13 and S14†) or in the solid state (Fig. S15 and S16†) produce typical europium-centred red luminescence, which results from indirect sensitization according to the antenna mechanism.[34] The initial ligand-centred $^1\pi^* \leftarrow {}^1\pi$ excitation is followed by a (probable)[35] intersystem crossing process, then **L1** → Eu and/or X → Eu energy transfers occur, thus leading to Eu($^5D_1$) and Eu($^5D_0$)-centred emissions.[34,35] The europium-centred emission bands recorded for [EuX$_3$dig] and [EuX$_3$**L1**] are diagnostic for the existence of low-symmetry tris-β-diketonates Eu(III) complexes with (i) Eu($^5D_1 \rightarrow {}^7F_J$) emissions being far less intense than for Eu($^5D_0 \rightarrow {}^7F_J$)[15a,33] and (ii) Eu($^5D_0 \rightarrow {}^7F_J$) emissions being

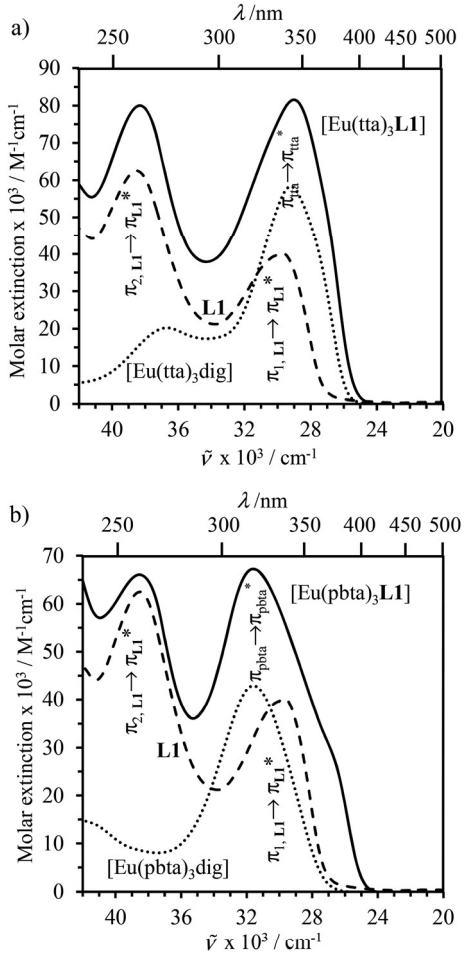

Fig. 12 Electronic absorption spectra recorded for (a) **L1** (dashed trace), [Eu(tta)$_3$dig] (dotted trace) and [Eu(tta)$_3$**L1**] (full trace), and (b) **L1** (dashed trace), [Eu(pbta)$_3$dig] (dotted trace) and [Eu(pbta)$_3$**L1**] (full trace) in CH_2Cl_2 + 10^{-6} m diglyme at 293 K. The absorption spectra were recorded for [Eu]$_{tot}$ = 10^{-5} m and corrected for partial dissociation in solution (Appendix 2).

dominated by the $2J + 1 = 5$ split components of the hypersensitive forced electric dipolar $^5D_0 \rightarrow {}^7F_2$ transition monitored around 16 320 cm^{-1} (Fig. 13 and S14†).[36] Only minor changes can be detected in terms of the relative intensities, splitting and energies for the Eu($^5D_0 \rightarrow {}^7F_J$) transitions when the diglyme in [EuX$_3$dig] is replaced with **L1** in [EuX$_3$**L1**]. However, the global quantum yields Φ^L_{Eu}, recorded upon UV-irradiation of the ligands while measuring the Eu-centered emission, rise by factors of 2 to 10 going from [EuX$_3$dig] (3% ≤ Φ^L_{Eu} ≤ 10%) to [EuX$_3$**L1**] (22% ≤ Φ^L_{Eu} ≤ 45%, Table S24†). These considerable global quantum yields are typical among tris-β-diketonate complexes, for which a systematic optimization may lead to 40–70% quantum yield values.[24,37]

More precisely, we note that the quantum yield Φ^L_{Eu} = 5(1)% obtained here for [Eu(hfa)$_3$dig] in dichloromethane is much lower than Φ^L_{Eu} = 35% reported for the same complex in ether : isopentane : ethanol (5 : 5 : 2).[38] In contrast, those obtained for [EuX$_3$**L1**] in the solid state (15–40%) are in line with Φ^L_{Eu} = 20–30% previously reported for closely related [Eu(hfa)$_3$**L**]

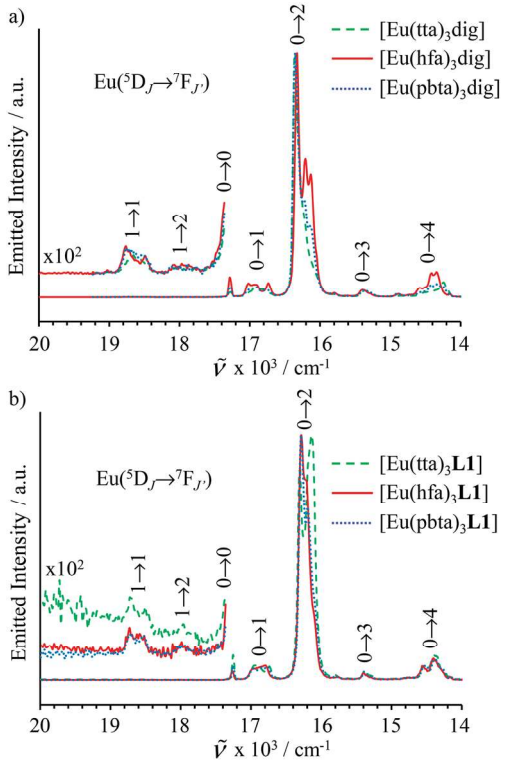

Fig. 13 Emission spectra recorded for (a) [EuX$_3$dig] with X = hfa ($\tilde{\nu}_{exc}$ = 29 850 cm^{-1}, [Eu]$_{tot}$ = 8.6 × 10^{-5} m, red full trace), X = tta ($\tilde{\nu}_{exc}$ = 28 570 cm^{-1}, [Eu]$_{tot}$ = 1.8 × 10^{-5} m, green dashed trace) and X = pbta ($\tilde{\nu}_{exc}$ = 29 850 cm^{-1}, [Eu]$_{tot}$ = 3.3 × 10^{-5} m, blue dotted trace) and for (b) [EuX$_3$**L1**] with X = hfa ($\tilde{\nu}_{exc}$ = 25 840 cm^{-1}, [Eu]$_{tot}$ = 4.0 × 10^{-5} m, red full trace), X = tta ($\tilde{\nu}_{exc}$ = 25 000 cm^{-1}, [Eu]$_{tot}$ = 5.5 × 10^{-4} m, green dashed trace) and X = pbta ($\tilde{\nu}_{exc}$ = 25 970 cm^{-1}, [Eu]$_{tot}$ = 6.1 × 10^{-5} m, blue dotted trace) in CH_2Cl_2 + 10^{-6} m diglyme at 293 K.

complexes where **L** is a terdentate N-donor ligand.[33] Although no detailed separation of radiative and non-radiative contributions to the various rate constants implied by the antenna mechanism are currently available, the observed mono-exponential millisecond range Eu(^{5}D0) lifetimes (Table S24†) reveal a reasonable protection of the Eu(III) emissive center against the harmonics of high-energy oscillators in these unsymmetrical complexes. Finally, the introduction of bis(hexyloxy)phenyl spacers in the binuclear complexes [Eu$_2$(hfa)$_6$**Lk**] (**Lk** = **L2–L4**) has a deleterious effect on the global quantum yields, which are reduced by one order of magnitude (2% ≤ Φ_{Eu}^{L} ≤ 5%) regarding those collected for the mononuclear analogues [Eu(hfa)$_3$**Lk**]. This specific effect was previously documented for related binuclear europium complexes[35a] and unambiguously assigned to a drastic reduction of the **Lk** → Eu(III) energy transfer rate constants when electron-donor groups are connected to the phenyl spacers. Our overview of the luminescence properties of [EuX$_3$dig], [Eu(hfa)$_3$**L1**] and [Eu$_2$(hfa)$_6$**Lk**] confirms that the replacement of symmetrical X = hfa ligands with unsymmetrical β-diketonate analogues (X = tta and pbta) does not dramatically impact the global photophysical properties of these complexes, which remain highly luminescent and therefore compatible with the preparation of strong red emissive lanthanidopolymers assuming that the thermodynamic metal loading is under control.

Conclusion

In line with theoretical predictions,[17] the replacement of symmetrical X = hfa with unsymmetrical X = tta or X = pbta β-diketonates in nine-coordinate neutral [LnX$_3$dig] lanthanide containers induces major changes in the thermodynamic loading of terdentate N$_3$ binding units. For both monomeric [LnX$_3$**L1**] and dimeric [Eu$_2$X$_6$**Lk**] complexes (**Lk** = **L2–L4**), the intrinsic affinity $f_{N_3,cond}^{LnX_3}$ depends on the residual positive charge borne by the metal. It increases in the order $f_{N_3,cond}^{Ln(tta)_3} \ll f_{N_3,cond}^{Ln(hfa)_3} \leq f_{N_3,cond}^{Ln(pbta)_3}$, which matches the electron-withdrawing character of the substituent groups located in the β-diketonate ligand (Fig. 8 and 11a). The supplementary inter-site repulsion operating in the dinuclear [Eu$_2$X$_6$**Lk**] complexes (**Lk** = **L2–L4**) is greatest for [Eu$_2$(pbta)$_6$**L3**] (Fig. 11b) with a remarkable anti-cooperative factor of $u_{L3}^{Eu(pbta)_3,Eu(pbta)_3} = 0.17(1)$, which translates into a repulsive free energy of $\Delta E_{L3}^{Eu(pbta)_3,Eu(pbta)_3} = 4.4(2)$ kJ mol^{-1}. The latter value is almost twice as large as the room temperature thermal energy.

Assuming a thought experiment in which (i) a linear infinite polymer **P2**^{N} ($N \rightarrow \infty$) based on the meta-substituted phenyl spacers, as found in **L3**, is at hand (Fig. 14 top), and (ii) the anti-cooperative factors $u_{L3}^{Eu(hfa)_3,Eu(hfa)_3} = 0.61(4)$ and $u_{L3}^{Eu(pbta)_3,Eu(pbta)_3} = 0.17(1)$ found for **L3** similarly operate in **P2**^{N}, the cluster expansion techniques[14] predict the appearance of an unprecedented identifiable 'plateau' in the binding isotherm of

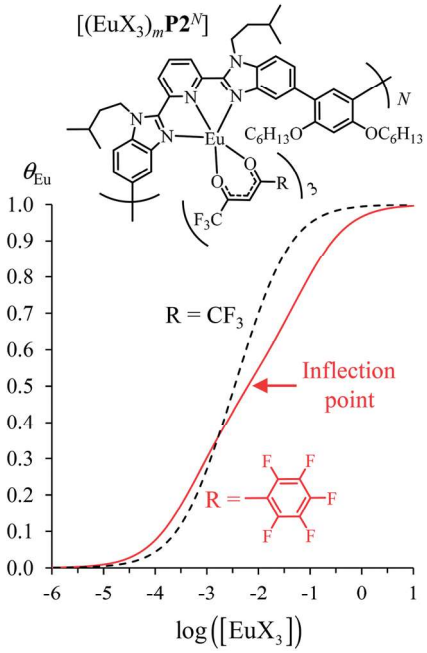

Fig. 14 Occupancy factors and binding isotherms computed for the loading of polymer **P2**^{N} ($N \rightarrow \infty$) in CH_2Cl_2 + 0.14 m diglyme at 293 K with [Eu(hfa)$_3$dig] (dotted black trace, $\Delta E_{L5^N}^{Eu(hfa)_3,Eu(hfa)_3} = \Delta E_{L3}^{Eu(hfa)_3,Eu(hfa)_3} = 1.2$ kJ mol^{-1}, Table S23†) and [Eu(pbta)$_3$dig] (full red trace, $\Delta E_{L5^N}^{Eu(pbta)_3,Eu(pbta)_3} = \Delta E_{L3}^{Eu(pbta)_3,Eu(pbta)_3} = 4.4$ kJ mol^{-1}, Table S23†).

the potential unsymmetrical linear $\{[Eu(pbta)_3]_m\mathbf{P2}^N\}$ lanthanidopolymer ($N \rightarrow \infty$, full red trace in Fig. 14), while its symmetrical analogue $\{[Eu(hfa)_3]_m\mathbf{P2}^N\}$ would exhibit only the standard stochastic distributions of metal ions (dashed black trace in Fig. 14). In other words, a predictable $|\mathbf{P2}^N|_{tot}/|Eu(pbta)_3|_{tot}$ stoichiometric ratio should provide an inflection point at $\theta_{Eu} = 0.5$, where the half-filled polymer $\{[Eu(pbta)_3]_{N/2}\mathbf{P2}^N\}$ is dominated by the formation of a microspecies, in which metal-occupied sites and metal-free sites strictly alternate (Fig. 1b bottom). The exact physical origin of this beneficial anti-cooperative effect remains elusive in the absence of quantitative access to solvation energies[39] and Born–Haber cycles,[17,22,40] but computational efforts are underway for unravelling the conditions required for exploiting this unprecedented effect for the preparation of highly organized metallopolymers.

Conflicts of interest

There are no conflicts to declare.

Acknowledgements

The Swiss National Science Foundation is gratefully acknowledged for financial support. The work performed in France was supported by La Ligue contre le Cancer, Cancéropôle Grand Ouest and INSERM.

References

1 A. Winter and U. S. Schubert, *Chem. Soc. Rev.*, 2016, **45**, 5311–5357.
2 Y. Yan, J. Zhang, L. Ren and C. Tang, *Chem. Soc. Rev.*, 2016, **45**, 5232–5263.
3 C.-L. Ho and W.-Y. Wong, *Coord. Chem. Rev.*, 2011, **255**, 2469–2502.
4 (*a*) M. O. Wolf, *Adv. Mater.*, 2001, **13**, 545–553; (*b*) M. O. Wolf, *J. Inorg. Organomet. Polym. Mater.*, 2006, **16**, 189–199.
5 J. M. Stanley and B. J. Holliday, *Coord. Chem. Rev.*, 2012, **256**, 1520–1530.
6 (*a*) J. Kido and Y. Okamoto, *Chem. Rev.*, 2002, **102**, 2357–2368; (*b*) A. de Bettencourt-Dias, *Dalton Trans.*, 2007, 2229–2241; (*c*) K. Binnemans, *Chem. Rev.*, 2009, **109**, 4283–4374.
7 (*a*) M. L. Huggins, *J. Chem. Phys.*, 1941, **9**, 440; (*b*) P. J. Flory, *J. Chem. Phys.*, 1941, **9**, 660–661; (*c*) *Polymer Blends*, ed. D. R. Paul and S. Newman, Academic Press, New York, San Francisco, London, 1978, vol. 2, pp. 25–32 and 116-121.
8 (*a*) C. Tschierske, *Ann. Rep. Progr. Chem. Ser. C*, 2001, **97**, 191–267; (*b*) E. Bialecka-Florjanczyk, *J. Phys. Chem. B*, 2006, **110**, 2582–2592; (*c*) C. Tschierske, *Top. Curr. Chem.*, 2012, **318**, 1–108.
9 (*a*) R. W. Corkery, *Curr. Opin. Colloid Interface Sci.*, 2008, **13**, 288–302; (*b*) J. Heine and K. Müller-Buschbaum, *Chem. Soc. Rev.*, 2013, **42**, 9232–9242.
10 (*a*) T. R. Cook, Y.-R. Zheng and P. J. Stang, *Chem. Rev.*, 2012, **113**, 734–777; (*b*) Y. Cui, Y. Yue, G. Qian and B. Chen, *Chem. Rev.*, 2012, **112**, 1126–1162; (*c*) Y. Cui, B. Chen and G. Qian, *Coord. Chem. Rev.*, 2014, **273–274**, 76–86.
11 O. Guillou, C. Daiguebonne, G. Calvez and K. Bernot, *Acc. Chem. Res.*, 2016, **49**, 844–856.
12 (*a*) J. B. Beck and S. J. Rowan, *J. Am. Chem. Soc.*, 2003, **125**, 13922–13923; (*b*) D. Knapton, P. K. Iyer, S. J. Rowan and C. Weder, *Macromolecules*, 2006, **39**, 4069–4075.
13 (*a*) D. A. Turchetti, P. C. Rodrigues, L. S. Berlim, C. Zanlorenzi, G. C. Faria, T. D. Z. Atvars, W.-H. Schreiner and L. C. Akcelrud, *Synth. Met.*, 2012, **162**, 35–43; (*b*) S. Basak, Y. S. L. V. Narayana, M. Baumgarten, K. Müllen and R. Chandrasekar, *Macromolecules*, 2013, **46**, 362–369; (*c*) Y. S. L. V. Narayana, S. Basak, M. Baumgarten, K. Müllen and R. Chandrasekar, *Adv. Funct. Mater.*, 2013, **23**, 5875–5880; (*d*) D. A. Turchetti, R. A. Domingues, C. Zanlorenzi, B. Nowacki, T. D. Z. Atvars and L. C. Akcelrud, *J. Phys. Chem. C*, 2014, **118**, 30079–30086; (*e*) S. Basak, M. A. Mohiddon, M. Baumgarten, K. Müllen and R. Chandrasekar, *Sci. Rep.*, 2015, **5**, 8406; (*f*) A. de Bettencourt-Dias and J. S. K. Rossini, *Inorg. Chem.*, 2016, **55**, 9954–9963.
14 (*a*) M. Borkovec, B. Jönsson and G. J. M. Koper, *Surf. Colloid Sci.*, 2001, **16**, 99–339; (*b*) G. Koper and M. Borkovec, *J. Phys. Chem. B*, 2001, **105**, 6666–6674; (*c*) M. Borkovec, J. Hamacek and C. Piguet, *Dalton Trans.*, 2004, 4096–4105; (*d*) M. Borkovec, G. J. M. Koper and C. Piguet, *Curr. Opin. Colloid Interface Sci.*, 2006, **11**, 280–289; (*e*) G. J. M. Koper and M. Borkovec, *Polymer*, 2010, **51**, 5649–5662.
15 (*a*) L. Babel, T. N. Y. Hoang, H. Nozary, J. Salamanca, L. Guénée and C. Piguet, *Inorg. Chem.*, 2014, **53**, 3568–3578; (*b*) T. N. Y. Hoang, Z. Wang, L. Babel, H. Nozary, M. Borkovec, I. Szilagyi and C. Piguet, *Dalton Trans.*, 2015, **44**, 13250–13260.
16 J. Hamacek, M. Borkovec and C. Piguet, *Chem.–Eur. J.*, 2005, **11**, 5217–5226.
17 L. Babel, T. N. Y. Hoang, L. Guénée, C. Besnard, T. A. Wesolowski, M. Humbert-Droz and C. Piguet, *Chem.–Eur. J.*, 2016, **22**, 8113–8123.
18 (*a*) A. Nonat, M. Regueiro-Figueroa, D. Esteban-Gomez, A. de Blas, T. Rodriguez-Blas, C. Platas-Iglesias and L. J. Charbonnière, *Chem.–Eur. J.*, 2012, **18**, 8163–8173; (*b*) A. Zaïm, S. V. Eliseeva, L. Guénée, H. Nozary, S. Petoud and C. Piguet, *Chem.–Eur. J.*, 2014, **20**, 12172–12182.
19 (*a*) U. S. Schubert and M. Heller, *Chem.–Eur. J.*, 2001, **7**, 5253–5259; (*b*) B. Liu, Y. Bao, F. Du, H. Wang, J. Tian and R. Bai, *Chem. Commun.*, 2011, **47**, 1731–1733; (*c*) Y. Yan, J. Zhang, L. Ren and C. Tang, *Chem. Soc. Rev.*, 2016, **45**, 5232–5263.
20 (*a*) C.-Y. Sun, X.-J. Zheng, X.-B. Chen and L.-P. Jin, *Inorg. Chim. Acta*, 2009, **362**, 325–330; (*b*) I. Hernandez, N. Pathumakanthar, P. B. Wyatt and W. P. Gillin, *Adv. Mater.*, 2010, **22**, 5356–5360.
21 (*a*) S. Hiraoka, M. Goda and M. Shionoya, *J. Am. Chem. Soc.*, 2009, **131**, 4592–4593; (*b*) K. Uemura, *Dalton Trans.*, 2017, **46**, 5474–5492.
22 (*a*) L. Onsager, *J. Am. Chem. Soc.*, 1936, **58**, 1486–1492; (*b*) D. V. Matyushov, *J. Chem. Phys.*, 2004, **120**, 1375–1382; (*c*) G. Schreckenbach, *Chem.–Eur. J.*, 2017, **23**, 3797–3803.

23 (*a*) W. J. Evans, D. G. Giarikos, M. A. Johnston, M. A. Greci and J. W. Ziller, *J. Chem. Soc., Dalton Trans.*, 2002, 520–526; (*b*) G. Malandrino, R. Lo Nigro, I. L. Fragala and C. Benelli, *Eur. J. Inorg. Chem.*, 2004, 500–509; (*c*) G. Malandrino and I. L. Fragala, *Coord. Chem. Rev.*, 2006, **250**, 1605–1620.

24 C. Freund, W. Porzio, U. Giovanella, F. Vignali, M. Pasini, S. Destri, A. Mech, S. Di Pietro, L. Di Bari and P. Mineo, *Inorg. Chem.*, 2011, **50**, 5417–5429.

25 S.-J. Kang, Y. S. Jung and Y. S. Sohn, *Bull. Korean Chem. Soc.*, 1997, **18**, 75–80.

26 SHAPE is a free software developed by M. Llunell, D. Casanova, J. Cirera, P. Alemany and S. Alvarez, available online at http://www.ee.ub.edu. For more information see (*a*) M. Pinsky and D. Avnir, *Inorg. Chem.*, 1998, **37**, 5575–5582; (*b*) D. Casanova, J. Cirera, M. Llunell, P. Alemany, D. Avnir and S. Alvarez, *J. Am. Chem. Soc.*, 2004, **126**, 1755–1763; (*c*) J. Cirera, E. Ruiz and S. Alvarez, *Chem.–Eur. J.*, 2006, **12**, 3162–3167.

27 V. Vallet, Z. Szabo and I. Grenthe, *Dalton Trans.*, 2011, **40**, 3154–3165.

28 A. Y. Rogachev, A. V. Nemukhin, N. P. Kuzmina and D. V. Sevastyanov, *Dokl. Chem.*, 2003, **389**, 87–91.

29 G. F. Gagabe, K. Satoh and K. Sawada, *Talanta*, 2011, **84**, 1047–1056.

30 (*a*) G. Richards, J. Osterwyk, J. Flikkema, K. Cobb, M. Sullivan and S. Swavey, *Inorg. Chem. Commun.*, 2008, **11**, 1385–1387; (*b*) S. S. Dudar', E. B. Sveshnikova and V. L. Ermolaev, *Opt. Spectrosc.*, 2008, **104**, 225–234; (*c*) Y. Hasegawa, S. Tamaki, S. Saitou, Z. Piskuła, H. Yajima, J. Noro and S. Lis, *Inorg. Chim. Acta*, 2009, **362**, 3641–3647; (*d*) M. R. Silva, P. Martin-Ramos, J. T. Coutinho, L. C. J. Pereira, V. Lavin, I. R. Martin, P. S. P. Silva and J. Martin-Gil, *Dalton Trans.*, 2015, **44**, 1264–1272.

31 G. Ercolani and L. Schiaffino, *Angew. Chem., Int. Ed.*, 2011, **50**, 1762–1768.

32 (*a*) K. Nakamoto, *J. Phys. Chem.*, 1960, **64**, 1420–1425; (*b*) C. Piguet, J.-C. G. Bünzli, G. Bernardinelli, C. Bochet and P. Froidevaux, *J. Chem. Soc., Dalton Trans.*, 1995, 83–97; (*c*) S. Xu, J. E. T. Smith and J. M. Weber, *Inorg. Chem.*, 2016, **55**, 11937–11943.

33 A. Zaïm, H. Nozary, L. Guénée, C. Besnard, J.-F. Lemonnier, S. Petoud and C. Piguet, *Chem.–Eur. J.*, 2012, **18**, 7155–7168.

34 (*a*) N. Sabbatini, M. Guardigli and I. Manet, in *Handbook on the Physics and Chemistry of Rare Earths*, ed. K. A. Gschneidner and L. Eyring, Elsevier Science, Amsterdam, 1996, vol. 23, pp. 69–120; (*b*) H. F. Brito, O. M. L. Malta, M. C. F. C. Felinto and E. E. S. Teotonio, *The Chemistry of Metal Enolates*, ed. J. Zabicky, John Wiley & Sons,Ltd, Chichester, 2009, ch. 3, pp. 131–184; (*c*) Y.-W. Yip, H. Wen, W.-T. Wong, P. A. Tanner and K.-L. Wong, *Inorg. Chem.*, 2012, **51**, 7013–7015; (*d*) M. Räsänen, H. Takalo, J. Rosenberg, J. Mäkelä, K. Haapakka and J. Kankare, *J. Lumin.*, 2014, **146**, 211–217.

35 (*a*) J.-F. Lemonnier, L. Guénée, C. Beuchat, T. A. Wesolowski, P. Mukherjee, D. H. Waldeck, K. A. Gogik, S. Petoud and C. Piguet, *J. Am. Chem. Soc.*, 2011, **133**, 16219–16234; (*b*) E. Kasprzycka, V. A. Trush, V. M. Amirkhanov, L. Jerzykiewicz, O. L. Malta, J. Legendziewicz and P. Gawryszewska, *Chem.–Eur. J.*, 2017, **23**, 1318–1330.

36 (*a*) C. Görller-Walrand and K. Binnemans, in *Handbook on the Physics and Chemistry of Rare Earths*, ed. K. A. Gschneidner and L. Eyring, Elsevier Science, Amsterdam, 1996, vol. 23, pp. 121–283; (*b*) G. F. de Sa, O. L. Malta, C. de Mello Donega, A. M. Simas, R. L. Longo, P. A. Santa-Cruz and E. F. da Silva Jr, *Coord. Chem. Rev.*, 2000, **196**, 165–195; (*c*) N. M. Shavaleev, S. V. Eliseeva, R. Scopelliti and J.-C. G. Bünzli, *Inorg. Chem.*, 2015, **54**, 9166–9173.

37 (*a*) K. Binnemans, in *Handbook on the Physics and Chemistry of Rare Earths*, ed. K. A. Gschneidner, J.-C. G. Bünzli and V. K. Pecharsky, Elsevier, North Holland, Amsterdam, 2005, vol. 35, pp. 107–272; (*b*) K. Miyata, Y. Hasegawa, K. Kuramochi, T. Nakagawa, T. Yokoo and T. Kawai, *Eur. J. Inorg. Chem.*, 2009, 4777–4785; (*c*) Z. Chen, F. Ding, F. Hao, M. Guan, Z. Bian, B. Ding and C. Huang, *New J. Chem.*, 2010, **34**, 487–494; (*d*) S. V. Eliseeva, D. N. Pleshkov, K. A. Lyssenko, L. S. Lepnev, J.-C. G. Bünzli and N. P. Kuzmina, *Inorg. Chem.*, 2011, **50**, 5137–5144; (*e*) A. I. S. Silva, V. F. C. Santos, N. B. D. Lima, A. M. Simas and S. M. C. Gonçalves, *RSC Adv.*, 2016, **6**, 90934–90943.

38 M. L. Bhaumik, *J. Chem. Phys.*, 1964, **40**, 3711–3715.

39 C. J. Cramer and D. G. Truhlar, *Acc. Chem. Res.*, 2008, **41**, 760–768.

40 N. Shimokhina, A. Bronowska and S. W. Homans, *Angew. Chem., Int. Ed.*, 2006, **45**, 6374–6376.